Projected Poleward migration of the Southern Ocean CO_2 sink region under high emissions

Precious Mongwe[1], Luke Gregor[2], Jerry Tjiputra[3], Judith Hauck[4], Takamitsu Ito[5], Christopher Danek[4], Marcello Vichi[6,7], Sandy Thomalla[1] and Pedro M. S. Monteiro[8]

[1]Southern Ocean Carbon Climate Observatory (SOCCO), CSIR, Cape Town, South Africa
[2]Environmental Physics, Institute of Biogeochemistry and Pollutant Dynamics, ETH Zurich, Zurich, Switzerland
[3]NORCE Norwegian Research Centre, Bjerknes Centre for Climate Research, Bergen, Norway
[4]Alfred-Wegener-Institut, Helmholtz Zentrum für Polar- und Meeresforschung, Bremerhaven, Germany
[5]Earth and Atmospheric Sciences, Georgia Institute of Technology, Atlanta, Georgia, USA
[6]Department of Oceanography, University of Cape Town, Cape Town, South Africa
[7]Marine and Antarctic Research centre for Innovation and Sustainability, University of Cape Town, Cape Town, South Africa
[8]School for Climate Studies, Stellenbosch University, Stellenbosch, South Africa

Supplementary Note 1: Mechanisms of CO_2 uptake in Sub-Antarctic region

The seasonal cycle of $(dpCO_2/dt)_{nonT}$ in the contemporary Sub-Antarctic region is broadly characterized by a maximum in mid-winter (JJA) and minima in late spring to early summer (NDJ) (Fig. 4e). The increase of $(dpCO_2/dt)_{nonT}$ from mid-autumn to winter coincides with the increase in dDIC/dt (Fig. 5e), surface cooling (Fig. 6i), and deepening of the MLD (Fig. 6c). As the surface ocean cools, the buoyancy flux weakens and MLD deepens. This stimulates the entrainment of the DIC-rich subsurface waters resulting in the increase of $dpCO_{2\ nonT}/dt$ during the cool seasons, peaking in winter (Fig. 4e). From early spring when light becomes available, the primary production removes ocean surface DIC to form organic matter. This decreases surface DIC concentrations (dDIC/dt < 0) and leads to the $(dpCO_2/dt)_{nonT}$ minima (Fig. 4e & 6a). NPP peak in ESMs coincides with a minimum in dDIC/dt (Fig. 6a & 4e). Furthermore, the timing of NPP peaking coincides with a minimum in the apparent oxygen utilization rate (dAOU/dt) (Fig. 6g, h). AOU is defined as the difference between oxygen at saturation (pre-formed estimate; O_{2sat}) and the in situ dissolved oxygen concentration (O_2); here, it is used to estimate near-surface (within the MLD) respiration. Negative dAOU/dt magnitude when NPP is high reflects oxygen production during photosynthesis, whereas positive dAOU/dt magnitudes can be used to roughly estimate the respiration or oxidation of organic matter back to DIC in the near-surface. Indeed, ESMs show positive dAOU/dt at the tail of NPP maxima, and, AOU and DIC rates are aligned which indicates respiration (Fig. 6). Moreover, we find that particularly large dAOU/dt magnitudes are shown by ESMs with extensive NPP magnitudes, (MPI models, Fig. S4 &); in these models, a significant amount of the organic matter formed during the growing season models is respired back to DIC within the MLD. It is worth noting that even if respiration occurs below the MLD, the MLD is still relatively shallow (~80m) when dAOU/dt is at its peak (Fig. 5). It is, therefore, unlikely that a significant amount of organic matter permanently leaves the winter mixed layer before it respire, it likely that a significant organic carbon is respired above the winter MLD.

No.	**Earth System Model**	**Country**	**Horizontal resolution**	**Vertical resolution**	**Reference**
1.	CanESM5	Canada	1^o x 1^o	z 45	Swart et al., 2019[1]
2.	CMCC-ESM2	Italy	1^o x 1^o	z 50	Lovato et al., 2022[2]
3.	CESM2-WACCM	USA	1^o x 1^o	z 60	Danabasoglu et al., 2020[3]
4.	IPSL-CM6A-LR	France	1^o x 1^o	z 75	Dufresne et al., 2013[4]
5.	NorESM2-LM	Norway	1^o x 1^o	z- ρ 53	Bentsen et al., 2013[5]
6.	MPI-ESM1-2-LR	Germany	1.5^o x 1.5^o	40	Mauritsen et al., 2019[6]
7.	MPI-ESM1-2-HR	Germany	0.4^o x 0.4^o	z 40	Müller et al., 2018[7]
8.	UKESM1-0-LL	UK	1^o x 1^o	Z 75	Sellar et al., 2019[8]
9.	AWI-CM1	Germany	0.25^o x 0.25^o		Semmler et al., 2020[16]

Supplementary table 1. The list of the nine Earth System models used in this study. For the vertical grid ρ means isopycnic and several symbols means hybrid

Abbreviated name	**Brief method description**	**Proxy variables**	**References**
JMA-MLR	A regional regression approach where MLR is applied to 44 defined regions	xCO2, SST, SSS, MLD, Chl-a, SLP, WIND	Iida et al. (2020)[10]
NIES-nn	A NN approach that uses no clustering or regions	MON, LAT, LON, SST, SSS, CHL	Zeng et al. (2014)[11]
CMEMS-LSCE-FFNN	Two-step NN that estimates seasonal variability and the anomalies there from	SST, SSS, SSH, MLD, Chl-a, xCO2	Denvil-Sommer et al. (2019)[12]
MPI-SOMFFN	A two-step approach that first clusters data with SOM, and then performs a regression per cluster using NN.	xCO2, SST, SSS, MLD, Chl-a	Landschützer et al. (2014)[13]
CSIR-ML6	An ensemble two-step cluster-regression approaches. Clustering is performed with K-means, and	xCO2, SST, SSS, MLD, Chl-a, WIND, MON	Gregor et al. (2019)[14]

	regression: NN, GBDT, and SVR.		
Jena-MLS	Mixed Layer Scheme: A bayesian approach that matches pCO2 observations to the mixed layer DIC budget.	SST, SSS, and other variables (see Fig 1 in reference)	Rödenbeck et al. (2013)[15]

Supplementary table 2. Details of observation-based surface pCO2 products collated in the SeaFlux ensemble product (Fay and Gregor et al. 2021). Note that the abbreviated names all contain the institution(s) and then an abbreviation for the method. Further, NN = neural network, SOM = self-organising map, MLR = multi-linear regression, GBDT = gradient boosted decision trees, SVR = support vector regression. For proxy variables, SST = sea surface temperature, SSS = sea surface salinity, SSH = sea surface height, MLD = mixed layer depth, Chl-a = Chlorophyll-a, SLP = sea level pressure, WIND = wind speed at 10m, xCO2 = atmospheric CO_2 concentration, LAT = latitude, LON = longitude, MON = month. Note that some of these variables have been transformed in the original study but have simplified for brevity in this table. Please see the original study for full details.

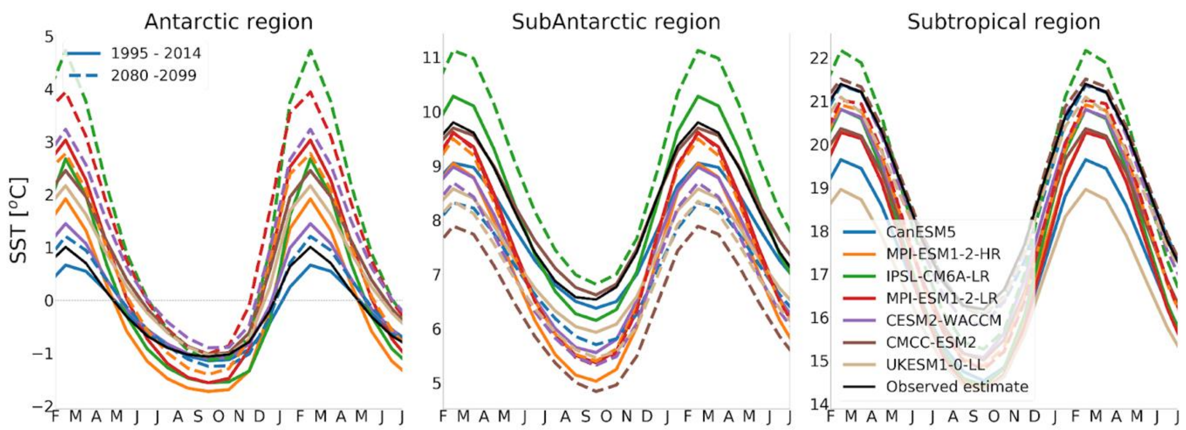

Supplementary figure 1. The seasonal cycle of sea surface temperature. The left panel is the Antarctic region, the middle panel is the Sub-Antarctic region, and the right is the subtropical region.

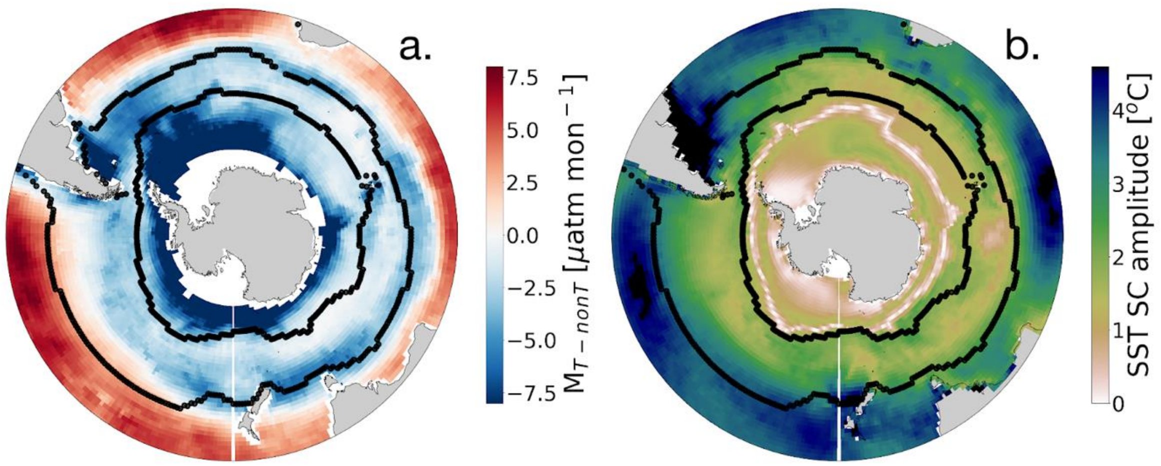

Supplementary figure 2. The left panel shows the annual mean of the observation-based estimate of MT-nonT (eq. 3), red (blue) denotes regions where the thermal (nonthermal) component is leading driving monthly pCO2 changes, and blue denotes nonthermal processes (biological and mixing) are leading the monthly pCO2 changes. The right panel shows the seasonal amplitude {summer (DJF) vs. winter (JJA)} of sea surface temperature in the Southern Ocean.

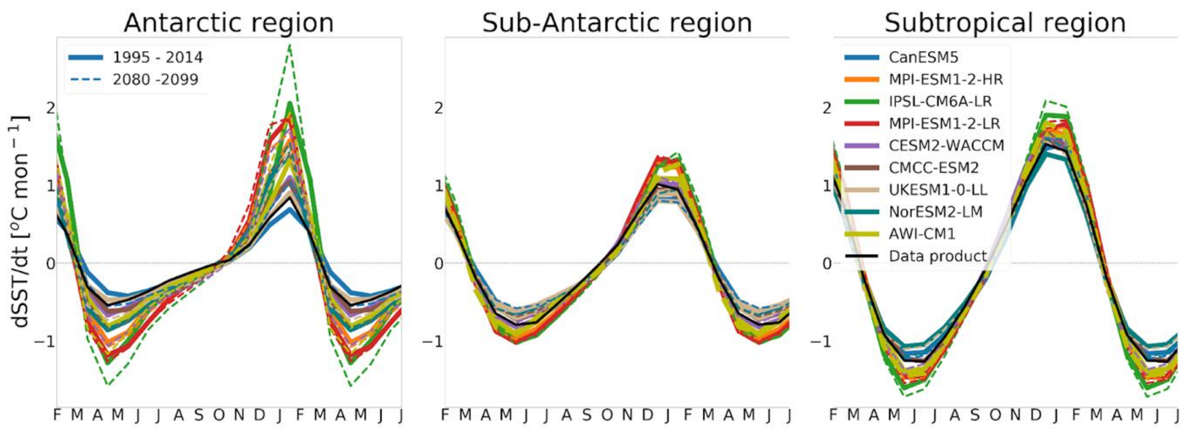

Supplementary figure 3. The seasonal cycle of the monthly rate of sea surface temperature. The left panel is the Antarctic region, the middle panel is the Sub-Antarctic region, and the right is the subtropical region.

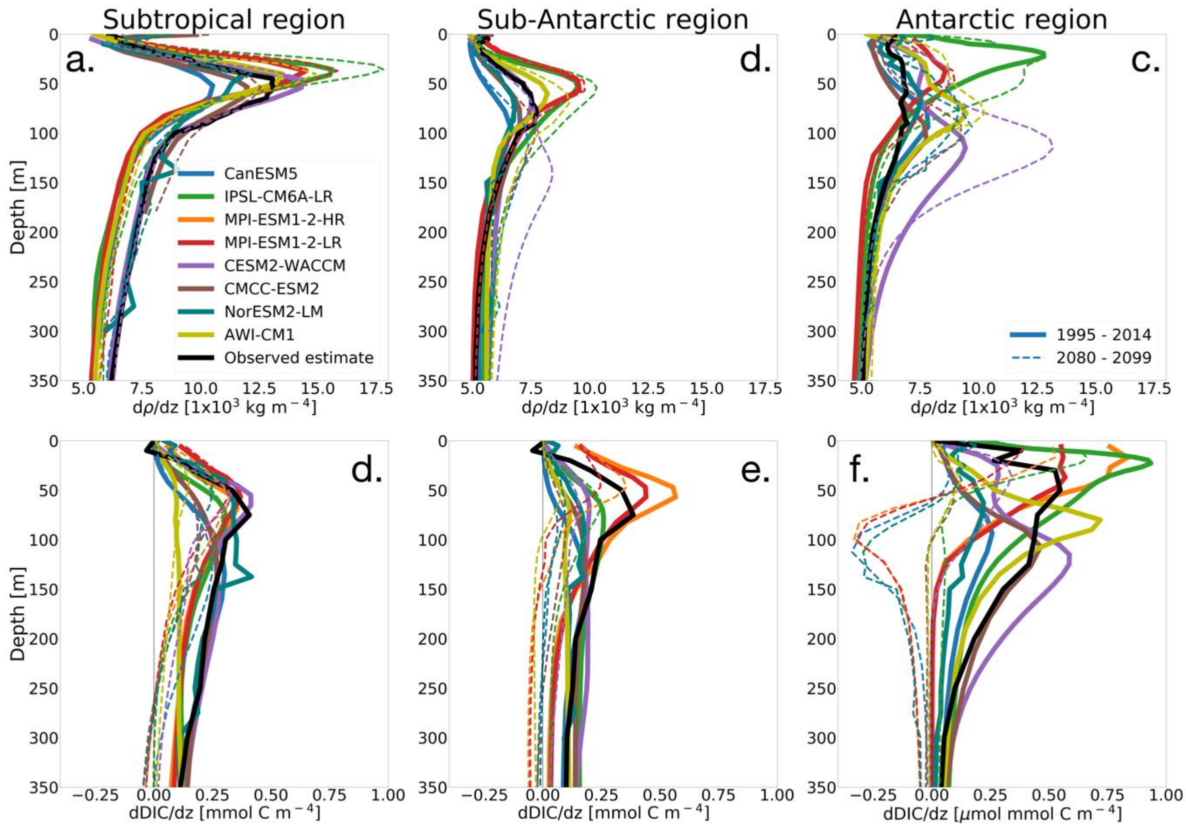

Supplementary figure 4. Vertical density gradient ($d\rho/dz$, top panel) and dissolved inorganic carbon vertical gradient (dDIC/dz, bottom panel) for Subtropical (left panel), Sub-Antarctic (middle panel) and Antarctic (right panel) regions. Solid lines depict the present climate (1995 – 2014) and dotted lines the end of the 21st century (2080 – 2099).

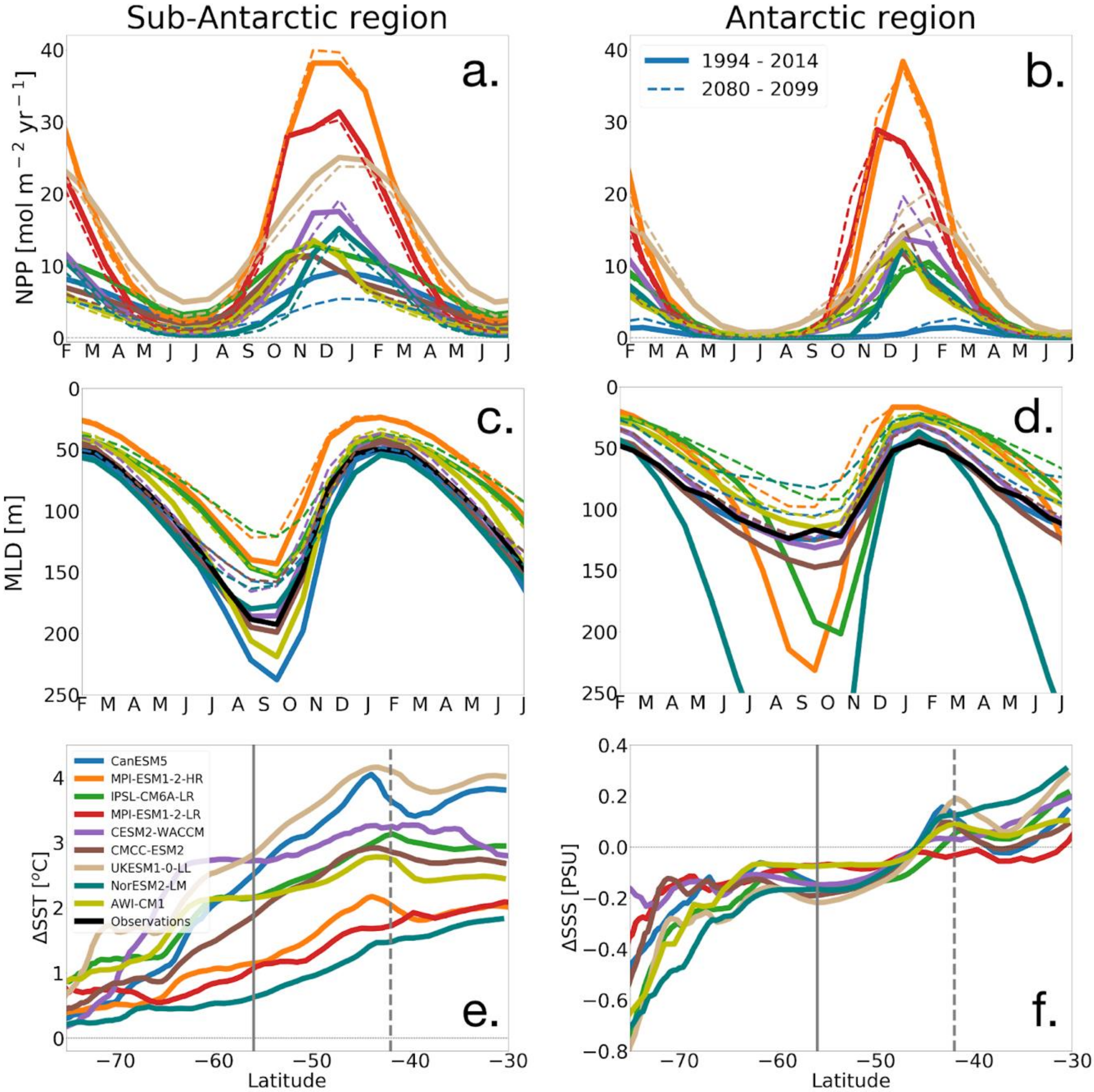

Supplementary figure 5. The seasonal cycle of net primary production (NPP, top panel), the seasonal cycle of the ocean mixed layer depth (MLD, second row panel). The solid lines are the present climate (1995 – 2014) and dotted lines are the end of the 21st century (2080 – 2099). The bottom panel shows zonal averages of sea surface temperature and surface salinity net change (2080-2099 vs 1995-2014).

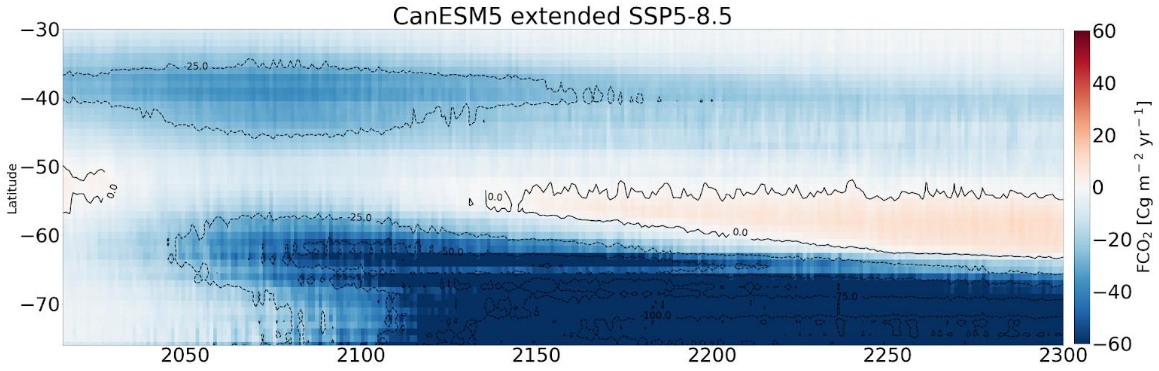

Supplementary figure 6. Annual and zonal mean air-sea CO_2 fluxes (FCO_2) south of 30° in CanESM5 for SSP5-8.5 climate scenario.

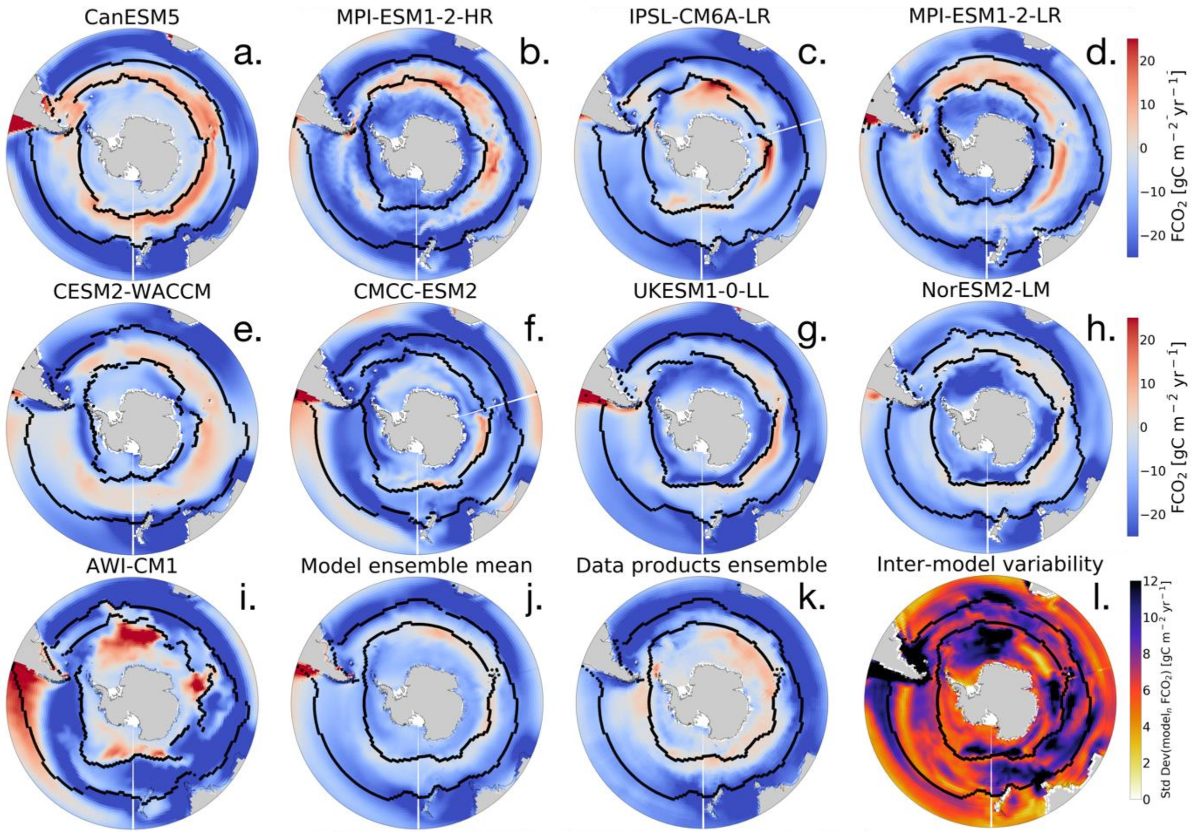

Supplementary figure 7. The climatological mean of air-sea CO_2 flux (FCO_2) in the Southern Ocean (south of 30°S) for nine CMIP6 ESMs for historical period (1995 - 2014), negative indicates flux into the ocean and positive outgassing for (a- i), the multi model mean (j), the ensemble mean of six pCO_2 products (k) and the ESM inter model variability (l), all given in gC m^{-2} yr^{-1}. The fronts are defined according to Orsi et al. (1995) as black lines with the Subtropical Front to the North and the Polar Front to the South. The zones are defined as the subtropical region north of the Subtropical Front (outer line), the Sub-Antarctic region between the two fronts and the Antarctic region to the south of the Polar Front (inner line).

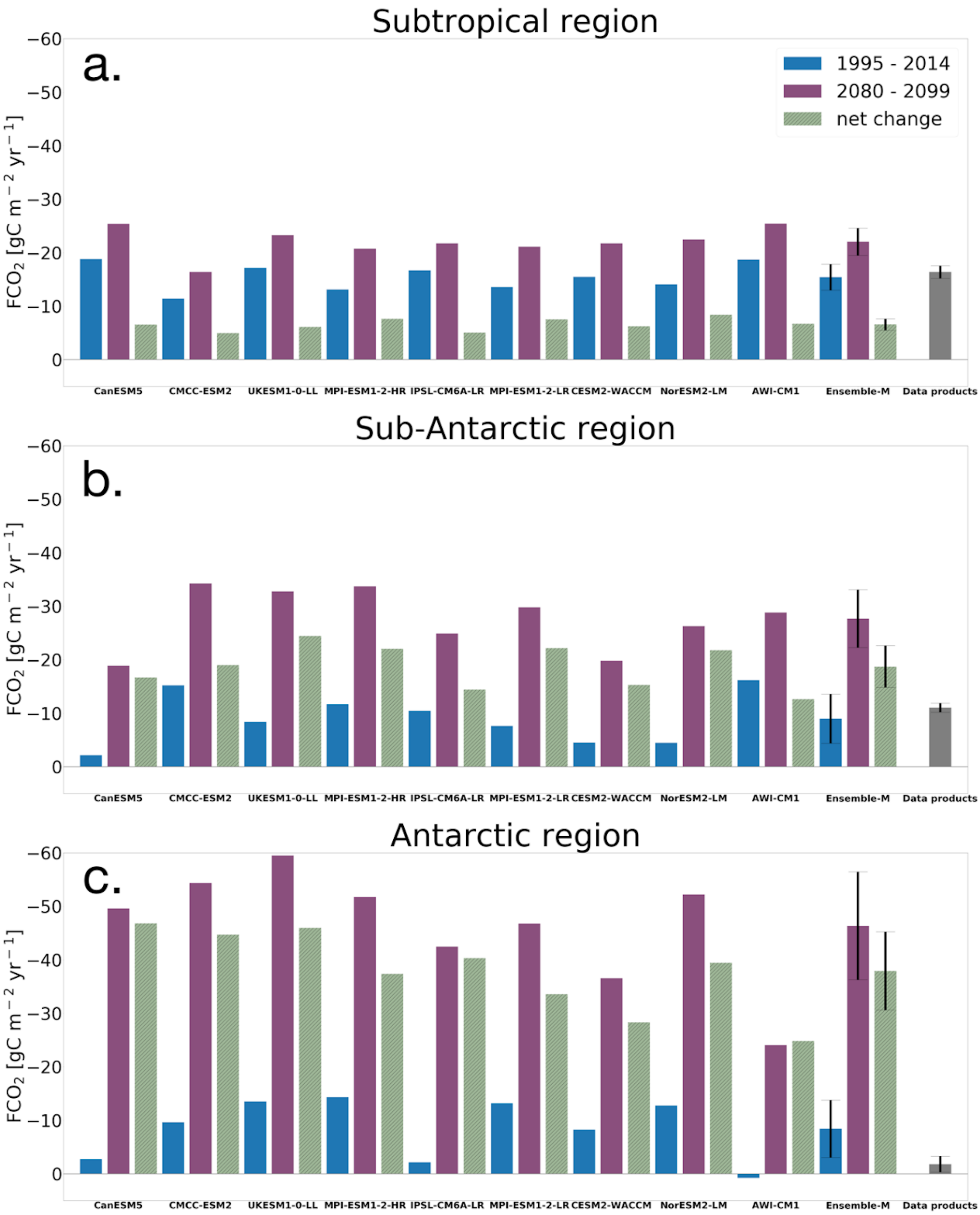

Supplementary figure 8. Annual mean air-sea CO_2 fluxes (FCO_2) in the Southern Ocean (south of 30°S) for nine CMIP6 ESMs, the multi model mean, and ensemble mean of six pCO_2 products, given in gC m^{-2} yr^{-1}. The error bars reflect the standard deviation.

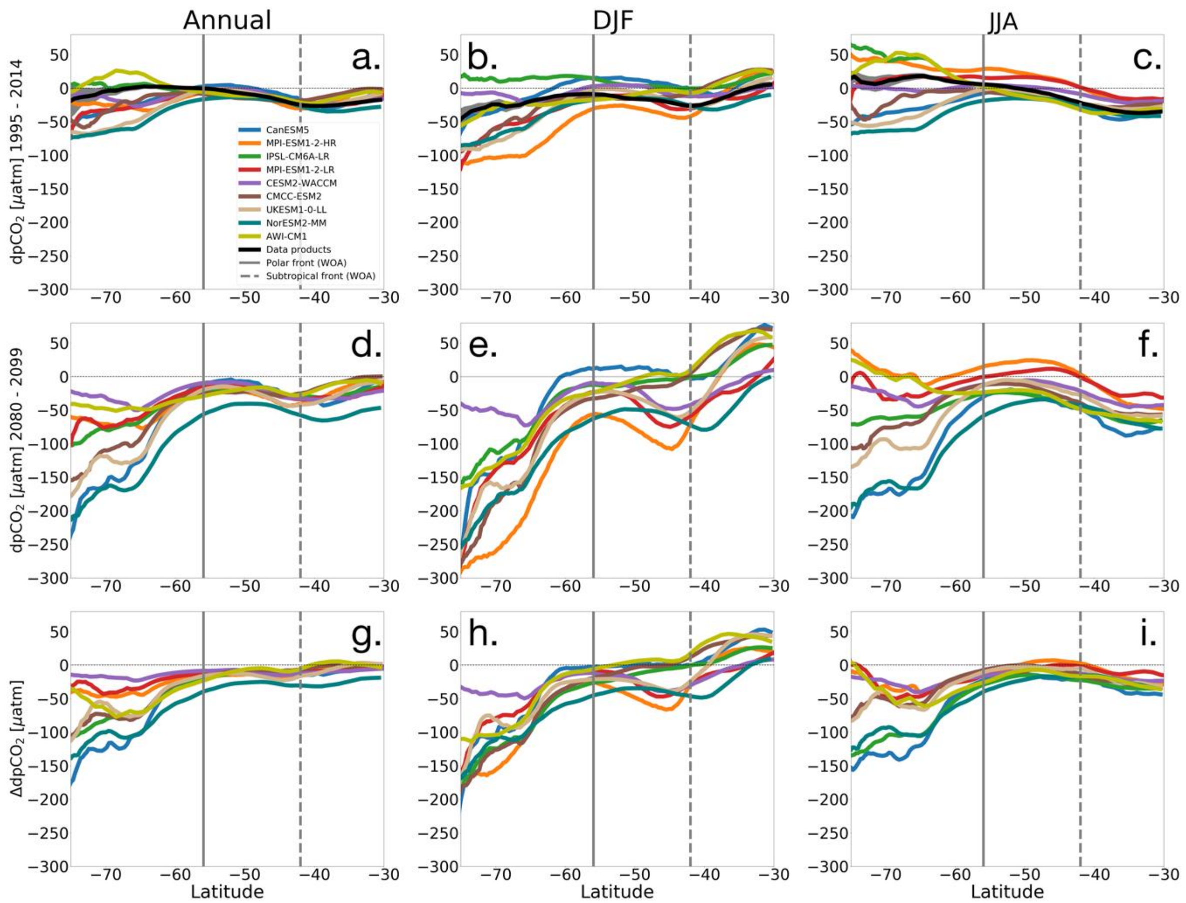

Supplementary figure 9. Zonally averaged $\Delta pCO2$ in the Southern Ocean (south of $30^{\circ}S$) for nine CMIP6 ESMs, and ensemble mean of six pCO_2 products, given in µatm units. The top panels show the present climate averages, middle panels show the end of the century (2080 – 2099) averages and net changes are shown in the bottom panel. The first, second, and third column depict the annual mean, the austral summer (DJF), and austral winter (JJA) averages, respectively. The vertical grey lines denote frontal positions, solid line the Polar Front and dotted the Subtropical Front.

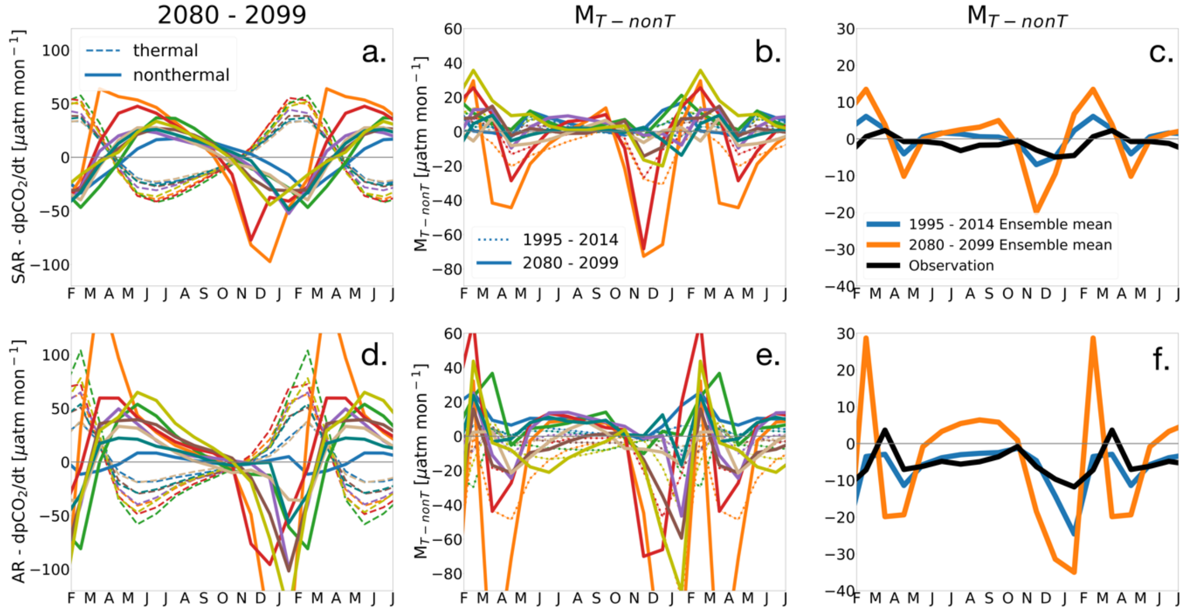

Supplementary figure 10. The seasonal cycle of the rate of change of the thermal ($dpCO_{2\ thermal}/dt$) and nonthermal ($dpCO_{2\ nonthermal}/dt$) ocean pCO_2 components for the present climate (left panel), the absolute difference between thermal and non-thermal components (middle panel; $M_{T\text{-}nonT}$) in the Sub-Antarctic region (SAZ, top panel) and Antarctic region (AZ, bottom panel). The right panel show the ensemble mean of the MT-nonT for present climate(blue), end of the 21st century (organge) and observations (black). The colors legend for each ESM in the first two columns follow the previous figure.

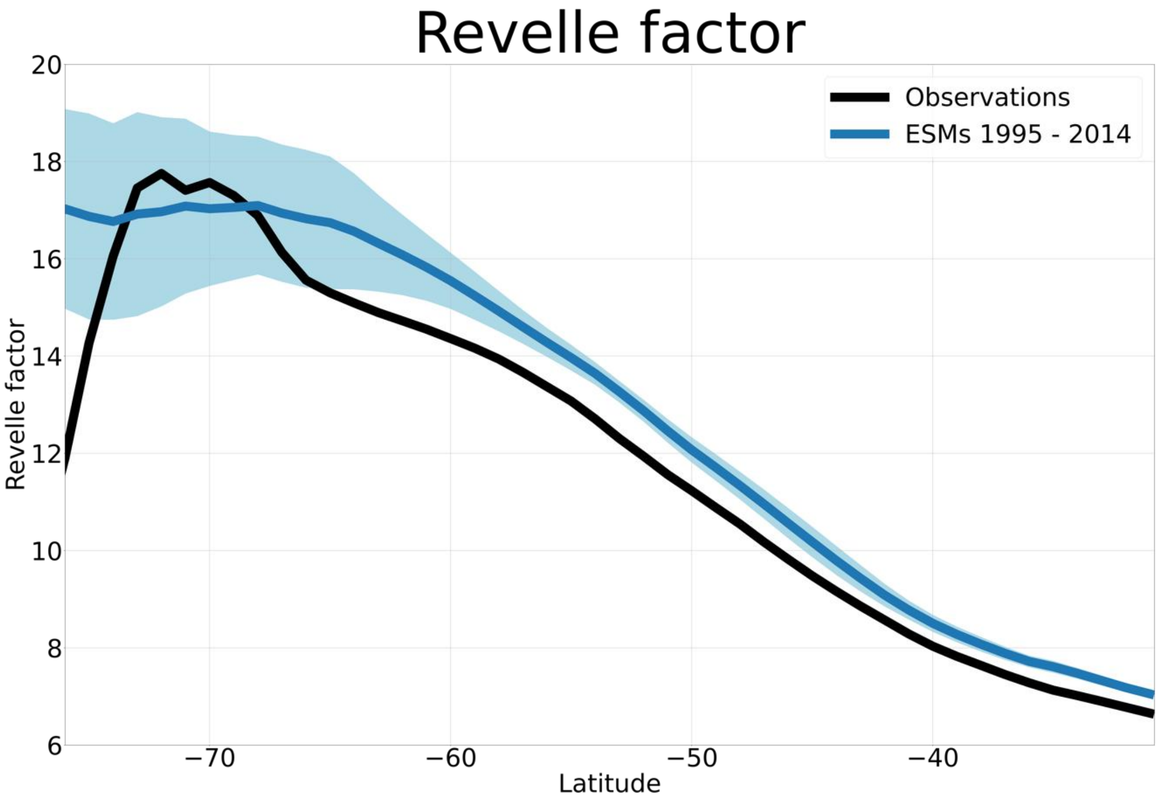

Supplementary figure 11. The Revelle factor ESMs ensemble (1995 – 2015, in blue) and the CSIR-ML6 data-product estimate in black. The shading show the inter-model variability, one standard deviation.

Supplementary References

1. Swart, N. C. *et al.* The Canadian Earth System Model version 5 (CanESM5.0.3). *Geosci Model Dev* **12**, 4823–4873 (2019).
2. Lovato, T. *et al.* CMIP6 Simulations With the CMCC Earth System Model (CMCC-ESM2). *J Adv Model Earth Syst* **14**, (2022).
3. Danabasoglu, G. *et al.* The Community Earth System Model Version 2 (CESM2). *J Adv Model Earth Syst* **12**, (2020).
4. Vial, J., Dufresne, J. L. & Bony, S. On the interpretation of inter-model spread in CMIP5 climate sensitivity estimates. *Clim Dyn* **41**, 3339–3362 (2013).
5. Bentsen, M. *et al.* The Norwegian Earth System Model, NorESM1-M – Part 1: Description and basic evaluation of the physical climate. *Geosci Model Dev* **6**, 687–720 (2013).

6. Mauritsen, T. *et al.* Developments in the MPI-M Earth System Model version 1.2 (MPI-ESM1.2) and Its Response to Increasing CO2. *J Adv Model Earth Syst* **11**, 998–1038 (2019).
7. Müller, W. A. *et al.* A Higher-resolution Version of the Max Planck Institute Earth System Model (MPI-ESM1.2-HR). *J Adv Model Earth Syst* **10**, 1383–1413 (2018).
8. Sellar, A. A. *et al.* UKESM1: Description and Evaluation of the U.K. Earth System Model. *J Adv Model Earth Syst* **11**, 4513–4558 (2019).
9. Semmler, T. *et al.* Simulations for CMIP6 With the AWI Climate Model AWI-CM-1-1. *J Adv Model Earth Syst* **12**, (2020).
10. Iida, Y., Takatani, Y., Kojima, A. & Ishii, M. Global trends of ocean CO2 sink and ocean acidification: an observation-based reconstruction of surface ocean inorganic carbon variables. *J Oceanogr* **77**, 323–358 (2021).
11. Zeng, J., Nojiri, Y., Landschützer, P., Telszewski, M. & Nakaoka, S. A global surface ocean fCO2 climatology based on a feed-forward neural network. *J Atmos Ocean Technol* **31**, 1838–1849 (2014).
12. Denvil-Sommer, A., Gehlen, M. & Vrac, M. Observation system simulation experiments in the Atlantic Ocean for enhanced surface ocean pCO2 reconstructions. *Ocean Science* **17**, 1011–1030 (2021).
13. Landschützer, P., Gruber, N., Bakker, D. C. E. & Schuster, U. Recent variability of the global ocean carbon sink. *Global Biogeochem Cycles* **28**, 927–949 (2014).
14. Gregor, L., Lebehot, A. D., Kok, S. & Scheel Monteiro, P. M. A comparative assessment of the uncertainties of global surface ocean CO2 estimates using a machine-learning ensemble (CSIR-ML6 version 2019a)-Have we hit the wall? *Geosci Model Dev* **12**, 5113–5136 (2019).
15. Rödenbeck, C. *et al.* Global surface-ocean pCO2 and sea-Air CO2 flux variability from an observation-driven ocean mixed-layer scheme. *Ocean Science* **9**, 193–216 (2013).
16. Semmler, T. *et al.* Simulations for CMIP6 With the AWI Climate Model AWI-CM-1-1. *J Adv Model Earth Syst* **12**, (2020).